Journal of Physical Chemistry and Functional Materials

Home Page of Journal: https://dergipark.org.tr/jphcfum

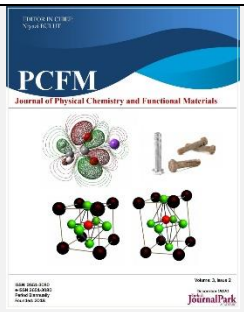

Population Analysis and UV-Vis Spectra of Dopamine Molecule Using Gaussian 09.

Lana O. Ahmed [a,c*] and Rebaz A. Omer[b,d]

[a]*Department of physics, Faculty of Science & Health, Koya University, Koya KOY45, Kurdistan Region – F.R. Iraq.*
[b]*Department of Chemistry, Faculty of Science & Health, Koya University, Koya KOY45, Kurdistan Region – F.R. Iraq*
[c] *Department of Physics, Faculty of Science, Firat University, 23169 Elazig, Turkey*
[d] *Department of Chemistry, Faculty of Science, Firat University, 23169 Elazig, Turkey*
** Corresponding author: E-mail: lana.omer@koyauniversity.org*

ABSTRACT

Dopamine has many important biological functions. In this article dopamine has been studied theoretically. We used Gaussian 09 software program with the B3LYP method at a 6-31G* basis set to optimize the geometrical structure of the dopamine molecule. Population analysis and UV-Vis absorption were registered and analyzed. The resulting natural bond orbital population analysis was observed in terms of charge density of the atoms and occupied valence shell orbitals by electrons with the energy of the occupation. Natural Bond Orbital Analysis which was searching for the Lewis and non-Lewis structure of the atoms in a molecular. The results showed dopamine is a Lewis structure. The Natural hybrid orbitals Analysis showed geometrical direction and the geometrical optimization of the title molecule. The Fukui functions have been reported to calculate bonding and antibonding with the strong stabilization of the atoms in a molecule. The convergence state for dopamine was recorded at excited 30 (n=30). Additionally, we applied and presented the solvation model effect on UV-Vis spectra. Six solvents (acetonitrile, chloroform, cyclohexane, dichloro-ethane, diethyl ether, and toluene) have been chosen and their wavelengths at maximum absorbance have been detected. The wavelength of the maximum peaks for dopamine was founded from 170 nm to 178.5 nm.

ARTICLE INFO

Keywords:
Dopamine,
DFT method,
Population analysis,
UV-Vis.
Solvation model.

Received: 4-November-2020,
Accepted: 14-November-2020
ISSN: 2651-3080

1. INTRODUCTION

Dopamine (DA) is an organic base, a benzene ring, and two hydroxyl side group consists of its molecule structure as illustrated in Figure 1 [1, 2] DA is a neurotransmitter [3] and a hormone in the human body [4, 5]. DA is produced in the ventral tegmental, substantia nigra, and hypothalamus of the brain [6] Also it is measured as vital elements in a brain, rewards system, and act of numerous drug abuses [7] DA has a vital role in the central nervous system [8]. Moreover, DA participates in several brain functions such as motor control, cognition, mood, sexual behavior, reward systems, and pain perception [9-11]. Parkinsonism and schizophrenia are two diseases that cause by the change of DA level [12, 13]. DA is the immune system's (IS) coregulator [14-19], organs, and tissues, for instance, kidney and adipose tissue [20-22]. Studies have been significantly increased since the 1980s, on monoamines, for example, DA, serotonin, and neuropeptides [23-26]. As well the structure analysis and molecular reactivity of the DA are important to understanding the ability to bonding receptor and mechanism in the body [27].

Hence there are two significant methods of population analysis and UV-Vis analysis to deal with the electronic transitions and orbital behaviors. Population analysis gives

information about molecular orbitals, various types of population analysis, and atomic charge assignments [28]. Furthermore, UV-Vis spectroscopy can determine the quantitative and qualitative evaluation of samples [29, 30]. Ultraviolet and visible radiation interacts with mater this leads to electronic transitions (moving electrons from the ground state with low energy to the excited state with higher energy state) [31]. Several factors will affect the electronic spectra of an organic molecule; one of them is the solvent effect [32]. Hydrogen bonding between the solute and the solvent molecules has a significant effect [33]. Different solvents will change peaks towards shorter or longer wavelengths [34].

In this study, DFT method at a 6-31G* basis was used, it is a chemical computational software program. It can model the electronic structure of any organic molecule [35]. Here, population analysis results have been discussed. Also, we will show the UV-Vis analysis [36-51] to deal with the geometrical structure of DA and its UV-Vis spectra. The six solvents were selected to see the effect of different solvents on the electronic spectra (UV-Visible spectra).

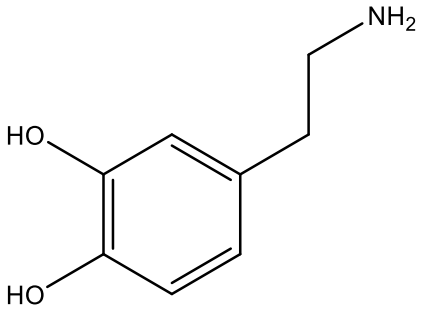

Figure 1: Structure of DA

2. COMPUTATIONAL METHODS

The structure of DA was designed by ChemBioDraw 12.0 (Figure 1). The geometrical structure of DA was optimized using Gaussian 09 software program and we applied density functional theory (DFT) at 6-31G* basis set. Population analysis method and UV-Vis analysis have been done for the DA molecular structure. We checked and ran different excited states n= 6, 12, 24, 30, and 36 to get convergence UV-Vis spectra to state. Then we chose UV-Vis spectra for state 30 and six solvents (acetonitrile, chloroform, cyclohexane, dichloro-ethane, diethyl ether, and toluene) have been selected to compare and see the differences between their maximum peaks for DA molecule.

3. RESULT AND DISCUSSION

3.1. Molecular Geometry

A DA chemical formula is $C_8H_{11}NO_2$ [52]. The molecule of DA consists of a benzene ring with two hydroxyl side groups, also one amine group attached by an ethyl chain [53]. The optimized molecular structure of DA is obtained from Gaussian 09 [54]as displayed in Figure 2

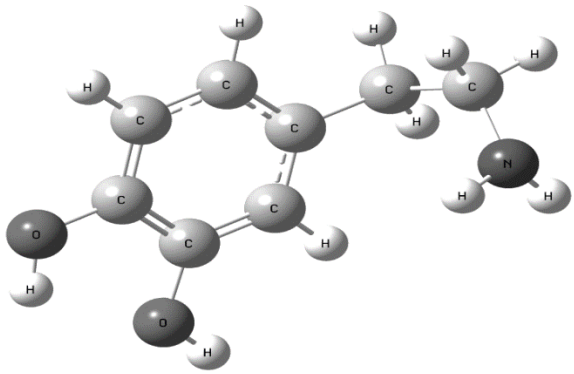

Figure 2: Geometry of the DA molecule

3.2. .Mulliken atomic charges

The calculation of Mulliken atomic charge is important in the quantum chemical, because of atomic charge effects on electronic structure, molecular polarization, dipole moment, and a lot of molecular properties. The distribution charge on the atomic molecule is advised to donor and acceptor pair of electrons. The atomic charge was using to electronegativity processes equalization and charge transmission in chemical reaction [55-57]. The calculation Mulliken atomic charge by DFT method on the basis set 6-31G* is showing in Table 1. It is mentioned that C3, C4, C5, C12, and C13 on title compounds exhibited a positive charge whereas C1, C2, and C6 were exhibit negative charge. H18 in a hydroxyl group was the maximum negative charge. The second maximum negative charge is the O8 and O7 in hydroxyl groups. The H22 was got the maximum positive charge this is due to that hydrogen was close to the nitrogen atoms. Also, H15 had the second maximum positive charge and it is closed to nitrogen atoms, after that nitrogen was the third maximum positive charge. The maximum positive charge was distributed on the hydrogen closed to the nitrogen atoms, but the maximum negative charge was distributed on the hydrogen closed to the oxygen.

Table 1: Mulliken atomic charges (*e*) calculated by DFT (6-31G*)

Atoms	DFT (6-31G*)	Atoms	DFT (6-31G*)
C1	-1.95957	C12	2.24763
C2	-1.23708	C13	3.15847
C3	0.11546	N14	3.00268
C4	0.77063	H15	3.33139
C5	0.02846	H16	2.11031
C6	-1.31731	H17	-1.68366
O7	-2.14456	H18	-3.65052
O8	-3.30137	H19	2.529
H9	0.50795	H20	2.46674
H10	0.66811	H21	2.97028
H11	-1.74715	H22	4.20596

3.3. Natural atomic orbital occupancies

Natural atomic orbitals (NAO) were produced from natural population analysis (NPA). The 121 NAO functions were listed in Table 2. The results give the information about the type of the momentum "lang" has s, px, py, and pz, the type of the orbitals include valence, core, Rydberg and hydrogenic, the occupancy of the orbitals and the energy of the orbitals. In the mentioned compound NAO 57 has the highest energy of oxygen orbitals of the natural molecular bonds, it is Rydberg (3s) valence shell orbitals occupied by $4.30*10^{-4}$ electrons, whereas NAO 55 records the lowest energy of oxygen that is equal to -18.9945 which is core (1s) valence shell orbitals and occupied by 1.99974 electrons. The occupancies of the core displayed the lower energy than Rydberg NAOs and valence NAOs. The role of natural molecular bonds orbitals telling the properties of the molecule.

Table 2: Natural atomic orbital occupancies

NAO	Atom	No	lang	Type(AO)	Occupancy	Energy (eV)	NAO	Atom	No	lang	Type(AO)	Occupancy	Energy (eV)
1	C	1	S	Cor(1S)	1.99853	-10.1141	61	O	7	py	Ryd(3p)	0.00177	1.17347
2	C	1	S	Val(2S)	0.82633	-0.13237	62	O	7	pz	Val(2p)	1.8717	-0.3278
3	C	1	S	Ryd(3S)	0.00118	0.98537	63	O	7	pz	Ryd(3p)	0.00116	0.98225
4	C	1	px	Val(2p)	0.79274	-0.05924	64	O	8	S	Cor(1S)	1.99976	-18.9618
5	C	1	px	Ryd(3p)	0.00792	0.87156	65	O	8	S	Val(2S)	1.67503	-0.89645
6	C	1	py	Val(2p)	1.08794	-0.06334	66	O	8	S	Ryd(3S)	1.60E-04	1.92595
7	C	1	py	Ryd(3p)	0.00532	0.89231	67	O	8	px	Val(2p)	1.49195	-0.30032
8	C	1	pz	Val(2p)	1.01093	-0.11306	68	O	8	px	Ryd(3p)	0.002	1.03857
9	C	1	pz	Ryd(3p)	0.00157	0.67852	69	O	8	py	Val(2p)	1.66973	-0.30409
10	C	2	S	Cor(1S)	1.99894	-10.0396	70	O	8	py	Ryd(3p)	0.00117	1.24959
11	C	2	S	Val(2S)	0.95491	-0.15627	71	O	8	pz	Val(2p)	1.85649	-0.30125
12	C	2	S	Ryd(3S)	8.70E-04	1.02112	72	O	8	pz	Ryd(3p)	0.00134	0.97518
13	C	2	px	Val(2p)	1.09704	-0.04671	73	H	9	S	Val(1S)	0.76082	0.06694
14	C	2	px	Ryd(3p)	0.0046	0.81364	74	H	9	S	Ryd(2S)	0.00182	0.57027
15	C	2	py	Val(2p)	1.1622	-0.06065	75	H	10	S	Val(1S)	0.75535	0.09592
16	C	2	py	Ryd(3p)	0.00484	0.9581	76	H	10	S	Ryd(2S)	0.00115	0.57235
17	C	2	pz	Val(2p)	1.043	-0.09922	77	H	11	S	Val(1S)	0.73932	0.10632
18	C	2	pz	Ryd(3p)	0.00126	0.67197	78	H	11	S	Ryd(2S)	0.00142	0.57216
19	C	3	S	Cor(1S)	1.99894	-10.0365	79	C	12	S	Cor(1S)	1.99913	-10.0446
20	C	3	S	Val(2S)	0.94402	-0.1493	80	C	12	S	Val(2S)	1.03769	-0.2323
21	C	3	S	Ryd(3S)	6.70E-04	1.04388	81	C	12	S	Ryd(3S)	7.30E-04	1.38999
22	C	3	px	Val(2p)	1.09671	-0.04708	82	C	12	px	Val(2p)	1.05601	-0.07065
23	C	3	px	Ryd(3p)	0.00384	0.85363	83	C	12	px	Ryd(3p)	0.00152	0.60328

24	C	3	py	Val(2p)	1.16763	-0.0553	84	C	12	py	Val(2p)	1.25309	-0.09168
25	C	3	py	Ryd(3p)	0.00477	1.00165	85	C	12	py	Ryd(3p)	0.00556	0.89553
26	C	3	pz	Val(2p)	1.0297	-0.09628	86	C	12	pz	Val(2p)	1.14685	-0.08437
27	C	3	pz	Ryd(3p)	9.70E-04	0.64549	87	C	12	pz	Ryd(3p)	0.00116	0.65139
28	C	4	S	Cor(1S)	1.99894	-10.0457	88	C	13	S	Cor(1S)	1.9992	-10.082
29	C	4	S	Val(2S)	0.87122	-0.13458	89	C	13	S	Val(2S)	1.0204	-0.22942
30	C	4	S	Ryd(3S)	0.00118	1.07774	90	C	13	S	Ryd(3S)	0.00179	1.30796
31	C	4	px	Val(2p)	1.06639	-0.05345	91	C	13	px	Val(2p)	1.17334	-0.08186
32	C	4	px	Ryd(3p)	0.00531	1.16099	92	C	13	px	Ryd(3p)	0.00332	0.74133
33	C	4	py	Val(2p)	1.07785	-0.05061	93	C	13	py	Val(2p)	0.9786	-0.06757
34	C	4	py	Ryd(3p)	0.00441	0.91895	94	C	13	py	Ryd(3p)	0.00321	0.63371
35	C	4	pz	Val(2p)	1.01938	-0.09356	95	C	13	pz	Val(2p)	1.08894	-0.06971
36	C	4	pz	Ryd(3p)	0.00281	0.75877	96	C	13	pz	Ryd(3p)	0.00398	0.6615
37	C	5	S	Cor(1S)	1.99887	-10.0452	97	N	14	S	Cor(1S)	1.99954	-14.1554
38	C	5	S	Val(2S)	0.94379	-0.15965	98	N	14	S	Val(2S)	1.37046	-0.53027
39	C	5	S	Ryd(3S)	9.60E-04	1.05015	99	N	14	S	Ryd(3S)	3.20E-04	1.36061
40	C	5	px	Val(2p)	1.09214	-0.066	100	N	14	px	Val(2p)	1.58935	-0.18759
41	C	5	px	Ryd(3p)	0.00381	0.81805	101	N	14	px	Ryd(3p)	0.00329	0.90639
42	C	5	py	Val(2p)	1.1763	-0.07426	102	N	14	py	Val(2p)	1.2855	-0.16926
43	C	5	py	Ryd(3p)	0.00469	0.97841	103	N	14	py	Ryd(3p)	0.00226	0.84226
44	C	5	pz	Val(2p)	1.08943	-0.11437	104	N	14	pz	Val(2p)	1.6648	-0.19693
45	C	5	pz	Ryd(3p)	0.00125	0.67925	105	N	14	pz	Ryd(3p)	0.00435	0.85748
46	C	6	S	Cor(1S)	1.99853	-10.1214	106	H	15	S	Val(1S)	0.61572	0.14381
47	C	6	S	Val(2S)	0.83086	-0.14448	107	H	15	S	Ryd(2S)	0.00192	0.59171
48	C	6	S	Ryd(3S)	0.00151	1.0098	108	H	16	S	Val(1S)	0.60671	0.15477
49	C	6	px	Val(2p)	0.99721	-0.0631	109	H	16	S	Ryd(2S)	0.00196	0.64204
50	C	6	px	Ryd(3p)	0.00659	0.91552	110	H	17	S	Val(1S)	0.49768	0.1037
51	C	6	py	Val(2p)	0.85519	-0.07248	111	H	17	S	Ryd(2S)	0.00146	0.59409
52	C	6	py	Ryd(3p)	0.0047	0.81489	112	H	18	S	Val(1S)	0.49097	0.132
53	C	6	pz	Val(2p)	1.05856	-0.12457	113	H	18	S	Ryd(2S)	0.00193	0.65682
54	C	6	pz	Ryd(3p)	9.40E-04	0.66996	114	H	19	S	Val(1S)	0.74926	0.08379
55	O	7	S	Cor(1S)	1.99974	-18.9945	115	H	19	S	Ryd(2S)	0.0022	0.66588
56	O	7	S	Val(2S)	1.67475	-0.91866	116	H	20	S	Val(1S)	0.75959	0.0782
57	O	7	S	Ryd(3S)	4.30E-04	1.79832	117	H	20	S	Ryd(2S)	0.00221	0.66478
58	O	7	px	Val(2p)	1.73675	-0.33952	118	H	21	S	Val(1S)	0.76169	0.09205
59	O	7	px	Ryd(3p)	0.00152	1.0985	119	H	21	S	Ryd(2S)	0.00216	0.65112
60	O	7	py	Val(2p)	1.441	-0.31771	120	H	22	S	Val(1S)	0.76162	0.08875
							121	H	22	S	Ryd(2S)	0.00199	0.63825

3.4. Natural Bond Orbital Analysis

The other result that obtained from the output results of the Natural Bond Orbital (NBO) Population analysis is natural bond orbital analysis. The NBO firstly searching for Lewis's structure. The results were summarized in table 3. Which included a variety of information for a cycle such as a threshold occupancy for a very good pair in a natural bond orbital, Lewis and non-Lewis natural bond orbitals, core number (CR), 2-Bond center (BD), 3-Bond center (3C), Lone pair (LP), low occupancy Lewis (L), high occupancy non-Lewis orbital (NL). The structure of the compounds was accepted Lewis structure if all orbitals exceed occupancy threshold and nonappearance from 1.90 electrons. For motion DA compounds the nitrogen atom has a higher cycle equal to eight with a higher occupancy Lewis and Lewis structure. Table 4 demonstrates the summary of the occupancies Lewis and non-Lewis structure with Rydberg, core, and valence shell contribution. Also, it shows the general description in a term of percentage for the natural Lewis structure for total electronic density. Generally, the DA compound presented the higher percentage of Lewis structure is equal to 97.967%. Moreover, table 4 describes the valance non-lewis orbitals which were equal to 1.909% and Rydberg non-lewis equal to 0.126%. Finally, the result demonstrated that DA was localized to the lewis model structure.

Table 3: Natural Bond Orbital Analysis

cycle	Occ. Thresh	Occupancies		Lewis Structure				Lower Occ (L)	High Occ (NL)
		Lewis	Non-Lewis	CR	BD	nC	LP		
1(1)	1.9	78.5542	3.4458	11	23	0	7	3	3
2(2)	1.9	78.5542	3.4458	11	23	0	7	3	3
3(1)	1.8	78.43556	3.56444	11	22	0	8	3	3
4(2)	1.8	78.43556	3.56444	11	22	0	8	3	3
5(1)	1.7	79.04742	2.95258	11	23	0	7	2	3
6(2)	1.7	79.04742	2.95258	11	23	0	7	2	3
7(1)	1.6	79.70975	2.29025	11	24	0	6	1	3
8(2)	1.6	80.33106	1.66894	11	25	0	5	0	3
9(3)	1.6	80.27996	1.72004	11	25	0	5	0	3
10(4)	1.6	79.70975	2.29025	11	24	0	6	1	3
11(5)	1.6	80.33106	1.66894	11	25	0	5	0	3
12(6)	1.6	80.27996	1.72004	11	25	0	5	0	3
13(7)	1.6	79.70975	2.29025	11	24	0	6	1	3
14(8)	1.6	80.33106	1.66894	11	25	0	5	0	3
15(9)	1.6	80.27996	1.72004	11	25	0	5	0	3
16(1)	1.5	79.36049	2.63951	11	23	0	7	0	5
17(2)	1.5	79.36049	2.63951	11	23	0	7	0	5
18(1)	1.6	80.33106	1.66894	11	25	0	5	0	3

Table 4: summary of Natural Bond Orbital Analysis

Core	21.99011 (99.955% of 22)
Valence Lewis	58.34096 (97.235% of 60)
Valence non-Lewis	1.56529 (1.909% of 82)
Rydberg non-Lewis	0.10365 (0.126% of 82)
Total non-Lewis	1.66894 (2.035% of 82)

3.5. Natural hybrid orbitals Analysis

From natural population analysis, one of its output results is natural hybrid analysis. The result expressions the comparison between the direction centerline with hybrid direction for two nuclei. This is useful to determine the deviation angle in a degree and bending of the bonds between two directions. The direction of the sp^{λ} hybrid is the specified terms of polar (θ) and azimuthal (φ) angles to vector describing *p*-component. In general, ($sp^{\lambda}d^{\mu}$) the direction hybrid determined exactly to angular amplitude. For instance, in the DA motion, the compound's result was shown in Table 5. The σ_{CN} for nitrogen hybrid bond (NBO 21) bents from a line of C-N center by 1.5^0, whereas the nitrogen hybrid of N-H bonds (NBOs 24, 25) bents to (2.5^0) and (2.7^0) respectively. The data in Table 5 was very useful for excepting the geometrical direction and resulting geometrical optimization.

3.6 Perturbation Theory of Energy Analysis

In perturbation energy analysis shows that the second-order estimates of bond or antibonding interaction on a basis of natural bond orbitals (NBO). This is done by all interaction possibility between donor, L (lewis types NBO, filled) and acceptor, NL (non-Lewis types, unfilled), and energy by 2nd order were important, it is estimated by perturbation theory. The interaction was lead to loss of occupancy from Lewis structure, localized NBOs to the non-Lewis orbitals, this is referred to as correction (delocalization) to the zero-order natural Lewis structure. For each NBO donor (*i*) and NBO acceptor (*j*), and energy stabilization *E*(2) for donor and acceptor was associated with $i \rightarrow j$ estimated as:

$$E(2) = \Delta E_{ij(2)} = q_i F(i,j)2/(\varepsilon_j - \varepsilon_i)$$

where *q*i is the donor orbital (1 for open-shell and 2 for closed-shell,), εi and εj are orbital energies and *F(i,j)* is the

Fock matrix element off-diagonal NBO. The DA molecule was shown in table 6. The *n*N → σ*CH interaction between lone pair of nitrogen and (NBO 44) and antiperiplanar antibonding (NBO 89) it is the strongest stabilization equal to 304.37 Kcal/mol. The heading table indicates the energy interaction exceeds defaults the threshold equal to 0.5 Kcal/mol

Table 5: NHO Directionality and "Bond Bending" (deviations from the line of nuclear centers)

[Thresholds for printing: angular deviation > 1.0 degree] hybrid p-character > 25.0% orbital occupancy > 0.10e																
NBO									Line of Centers		Hybrid 1			Hybrid 2		
									Theta	Phi	Theta	Phi	Dev	Theta	Phi	Dev
1	BD	(	1)	C	1	-	C	2	88.1	238.7	85.8	244.8	6.5	90.6	55.5	3.5
2	BD	(	2)	C	1	-	C	2	88.1	238.7	161.6	322.2	89.8	161.7	323.5	89.8
3	BD	(	1)	C	1	-	C	6	107	118.6	106.1	113.1	5.3	72.3	303.9	5.1
5	BD	(	1)	C	2	-	C	3	104.9	180.4	104.1	184.2	3.8	74.5	357	3.3
6	BD	(	1)	C	2	-	H	11	73.2	299.4	73.3	298.2	1.2	--	--	--
7	BD	(	1)	C	3	-	C	4	107.1	119.2	107.1	121.8	2.5	73.2	296.5	2.6
8	BD	(	2)	C	3	-	C	4	107.1	119.2	161.8	323	89.6	162.2	321.2	90.5
10	BD	(	1)	C	4	-	C	5	91.7	58.2	92.6	60.6	2.5	89	235.7	2.6
11	BD	(	1)	C	4	-	C	12	102.6	180.3	104.5	180.5	1.8	--	--	--
12	BD	(	1)	C	5	-	C	6	75.2	0.2	75.9	4.4	4.1	105.9	174	6.1
13	BD	(	2)	C	5	-	C	6	75.2	0.2	161.4	322.1	90	161.4	322	89.9
15	BD	(	1)	C	6	-	O	7	90.5	53.9	91.6	57.1	3.4	90.4	231.2	2.8
16	BD	(	1)	O	7	-	H	17	109.2	120.1	108.8	116.1	3.8	--	--	--
17	BD	(	1)	O	8	-	H	18	95.6	69	94.2	64.3	5	--	--	--
18	BD	(	1)	C	12	-	C	13	37.7	162.8	--	--	--	142.5	346.8	2.4
19	BD	(	1)	C	12	-	H	19	112.5	253.9	113.6	253.6	1.1	--	--	--
20	BD	(	1)	C	12	-	H	20	134.5	106.2	135.7	106.7	1.2	--	--	--
21	BD	(	1)	C	13	-	N	14	64.3	83.2	65.2	82.5	1.1	114.7	261.9	1.5
22	BD	(	1)	C	13	-	H	21	46.4	283.7	44.8	283.2	1.6	--	--	--
23	BD	(	1)	C	13	-	H	22	106.3	185.9	105.2	184.9	1.5	--	--	--
24	BD	(	1)	N	14	-	H	15	122	112.5	119.5	112.7	2.5	--	--	--
25	BD	(	1)	N	14	-	H	16	63.8	10.5	61.7	12.5	2.7	--	--	--
37	LP	(	1)	O	7				--	--	75	2.9	--	--	--	--
38	LP	(	2)	O	7				--	--	20.3	141.4	--	--	--	--
39	LP	(	1)	O	8				--	--	72.3	307.2	--	--	--	--
40	LP	(	2)	O	8				--	--	18.4	141.8	--	--	--	--
41	LP	(	1)	N	14				--	--	39.4	181.5	--	--	--	--
98	BD	*(	2)	C	1	-	C	2	88.1	238.7	161.6	322.2	89.8	161.7	323.5	89.8
104	BD	*(	2)	C	3	-	C	4	107.1	119.2	161.8	323	89.6	162.2	321.2	90.5
109	BD	*(	2)	C	5	-	C	6	75.2	0.2	161.4	322.1	90	161.4	322	89.9

3.1. UV- Vis Analysis

UV-Vis spectroscopy is a very simple method used to examine the structural changes and complex formation [50]. Time-dependent (TD) B3LYP method with 6-31G* basis set was calculated to obtain UV-Vis spectra for DA molecules. The absorption spectrum has been represented for n=6, 12, 24, 30, and 36 as in figures 3, 4, 5, 6, and 7 respectively. From the figures, the x-axis shows the wavelength in nanometers and the y-axis shows the absorbance. As we can see, there is a similarity between graphs 6 and 7. It means that there is a convergence state at excited state 30 (n=30). According to the mentioned figures (6 and 7), the wavelength of the maximum peak for both of them is 167nm.

.**Table 6.** Second-Order Perturbation Theory Analysis of Fock Matrix in NBO Basis

The threshold for printing: 0.50 kcal/mol																			
	Donor NBO (i)								Acceptor NBO (j)								E (2) Kcal/ mol	E (j) –E (i) a.u.	F (I,j) a.u.
1	BD	(	1)	C	1	-	C	2	/45.	BD*(	1)	O	8	-	H	18	1.7	1.12	0.039
2	BD	(	2)	C	1	-	C	2	/46.	BD*(	2)	C	5	-	C	6	21.73	0.27	0.07
3	BD	(	1)	C	1	-	C	6	/47.	BD*(	1)	O	7	-	H	17	1.93	1.11	0.041
4	BD	(	1)	C	1	-	O	8	/48.	BD*(	1)	C	5	-	C	6	1.63	1.46	0.044
5	BD	(	1)	C	2	-	C	3	/49.	BD*(	1)	C	4	-	C	12	3.26	1.1	0.053
6	BD	(	1)	C	2	-	H	11	/50.	BD*(	1)	C	3	-	C	4	3.62	1.09	0.056
7	BD	(	1)	C	3	-	C	4	/51.	BD*(	1)	C	12	-	H	20	0.6	1.12	0.023
8	BD	(	2)	C	3	-	C	4	/52.	BD*(	1)	C	12	-	H	20	1.04	0.68	0.026
9	BD	(	1)	C	3	-	H	10	/53.	BD*(	1)	C	4	-	C	5	4.06	1.07	0.059
10	BD	(	1)	C	4	-	C	5	/54.	BD*(	1)	C	12	-	H	19	0.58	1.13	0.023
11	BD	(	1)	C	4	-	C	12	/55.	BD*(	1)	C	12	-	H	19	0.69	1.05	0.024
12	BD	(	1)	C	5	-	C	6	/56.	BD*(	1)	C	5	-	H	9	1.51	1.16	0.038
13	BD	(	2)	C	5	-	C	6	/57.	BD*(	2)	C	3	-	C	4	18.21	0.3	0.068
14	BD	(	1)	C	5	-	H	9	/58.	RY*(	1)	C	4				1.34	1.7	0.043
15	BD	(	1)	C	6	-	O	7	/59.	BD*(	1)	C	5	-	C	6	0.86	1.47	0.032
16	BD	(	1)	O	7	-	H	17	/60.	RY*(	1)	C	6				1.28	1.67	0.041
17	BD	(	1)	O	8	-	H	18	/61.	BD*(	1)	C	1	-	C	2	4.61	1.31	0.07
18	BD	(	1)	C	12	-	C	13	/62.	RY*(	3)	C	4				1.38	1.38	0.039
18	BD	(	1)	C	12	-	C	13	/63.	BD*(	1)	C	12	-	H	20	0.57	1.01	0.021
19	BD	(	1)	C	12	-	H	19	/64.	BD*(	2)	C	3	-	C	4	0.75	0.53	0.02
20	BD	(	1)	C	12	-	H	20	/65.	BD*(	1)	C	13	-	H	21	2.33	0.94	0.042
21	BD	(	1)	C	13	-	N	14	/66.	RY*(	1)	C	12				0.71	1.62	0.03
22	BD	(	1)	C	13	-	H	21	/67.	BD*(	1)	N	14	-	H	15	3.46	0.97	0.052
23	BD	(	1)	C	13	-	H	22	/68.	BD*(	1)	C	4	-	C	12	3.25	0.91	0.049
24	BD	(	1)	N	14	-	H	15	/69.	BD*(	1)	C	13	-	H	21	1.89	1.07	0.04
25	BD	(	1)	N	14	-	H	16	/70.	BD*(	1)	C	13	-	H	22	1.92	1.07	0.041
26	CR	(	1)	C	1				/71.	RY*(	2)	C	2				1.87	10.81	0.127
27	CR	(	1)	C	2				/72.	BD*(	1)	C	3	-	H	10	0.56	10.51	0.069
28	CR	(	1)	C	3				/73.	RY*(	1)	C	2				0.65	11.15	0.076
29	CR	(	1)	C	4				/74.	BD*(	1)	C	5	-	H	9	0.61	10.49	0.072
30	CR	(	1)	C	5				/75.	RY*(	2)	C	4				2.51	10.97	0.148
31	CR	(	1)	C	6				/76.	BD*(	1)	C	1	-	O	8	0.59	10.43	0.07
32	CR	(	1)	O	7				/77.	RY*(	2)	C	6				0.84	19.87	0.116
33	CR	(	1)	O	8				/78.	RY*(	1)	C	1				1.97	19.86	0.177
34	CR	(	1)	C	12				/79.	BD*(	1)	C	4	-	C	5	0.58	10.61	0.071
35	CR	(	1)	C	13				/80.	RY*(	3)	C	12				0.75	11.22	0.082
36	CR	(	1)	N	14				/81.	RY*(	1)	H	16				0.59	14.79	0.084
37	LP	(	1)	O	7				/82.	RY*(	1)	C	6				2.47	1.51	0.055
38	LP	(	2)	O	7				/83.	BD*(	2)	C	5	-	C	6	23.48	0.34	0.087
39	LP	(	1)	O	8				/84.	BD*(	1)	C	1	-	C	6	6.04	1.12	0.074
40	LP	(	2)	O	8				/85.	BD*(	2)	C	1	-	C	2	26.9	0.33	0.09
41	LP	(	1)	N	14				/86.	BD*(	1)	C	12	-	C	13	10.75	0.59	0.071
42	BD	*(	2)	C	1	-	C	2	/87.	RY*(	4)	C	1				1.31	0.63	0.058
43	BD	*(	2)	C	3	-	C	4	/88.	BD*(	1)	C	12	-	C	13	2.1	0.32	0.051
44	BD	*(	2)	C	5	-	C	6	/89.	BD*(	2)	C	1	-	C	2	304.37	0.01	0.083

3.1. Solvation Model of UV-Vis Analysis

Figures 8, 9, 10, 11, 12, and 13 demonstrated the spectra of DA using some solvation (acetonitrile, chloroform, cyclohexane, dichloro-ethane, diethyl ether, and toluene) of UV-Vis respectively. As indicated in the graph, acetonitrile solvation has the greatest value (178.5 nm). The smallest wavelength has been obtained by cyclohexane solvation which is 170 nm. Meanwhile, the wavelength of the maximum peak for dichloro-ethane and toluene can be found at 176.5 nm and 171 nm respectively. Hence, chloroform and diethyl ether have the same wavelength (173.5 nm) at the maximum peak.

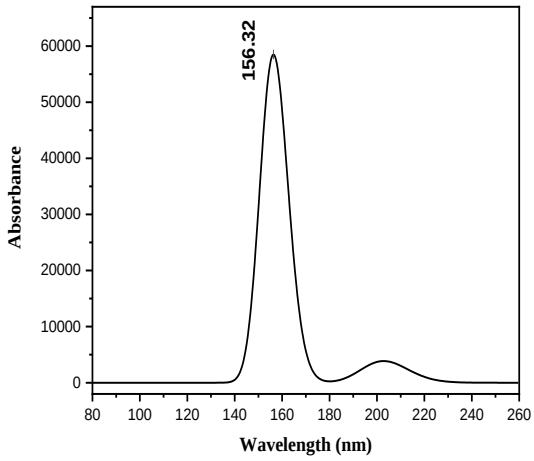

Figure 3: UV spectra for n=6

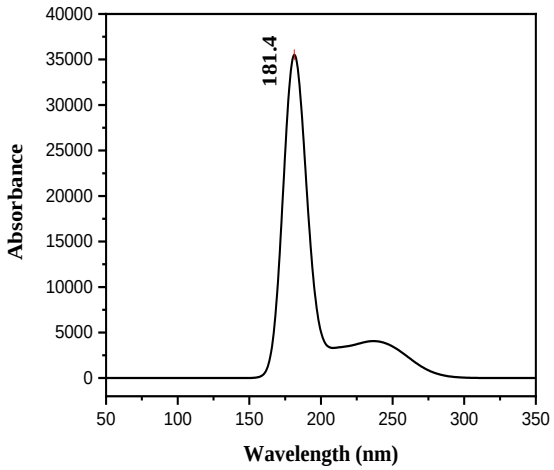

Figure 4: UV spectra for n=12

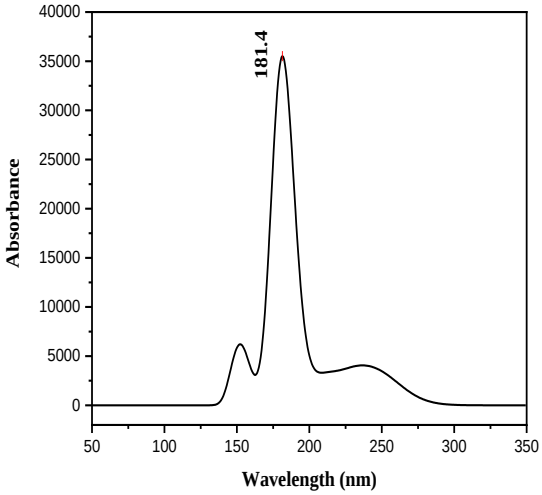

Figure 5: UV spectra for n=24

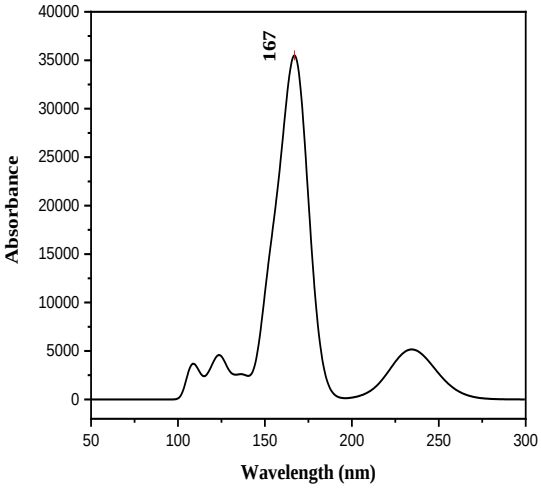

Figure 6: UV spectra for n=30

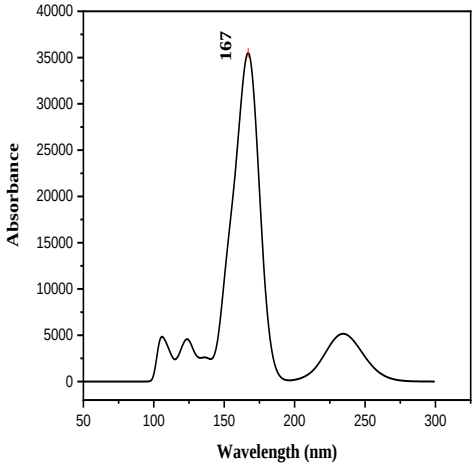

Figure 7: UV spectra for n=36

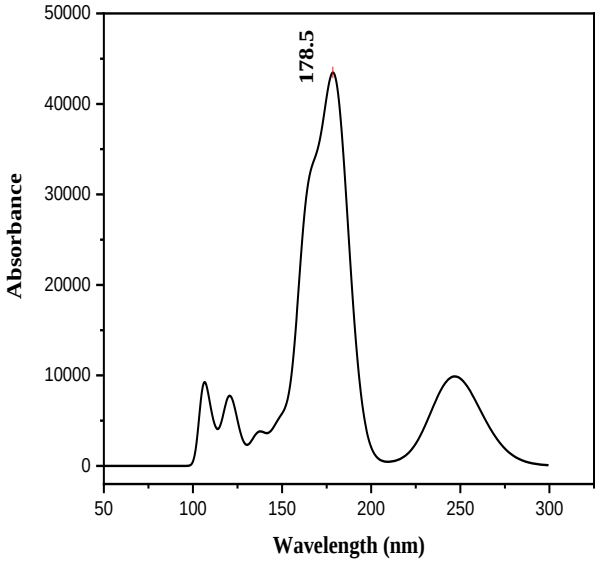

Figure 8: UV-Vis spectra with acetonitrile solvation.

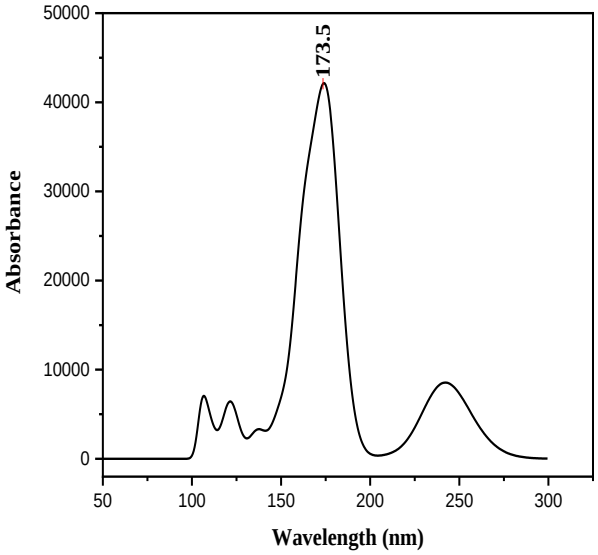

Figure 9: UV-Vis spectra with chloroform solvation.

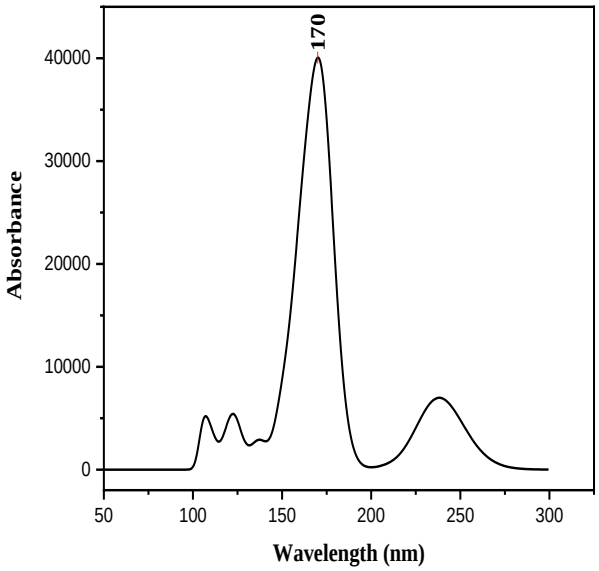

Figure 10: UV-Vis spectra with cyclohexane solvation.

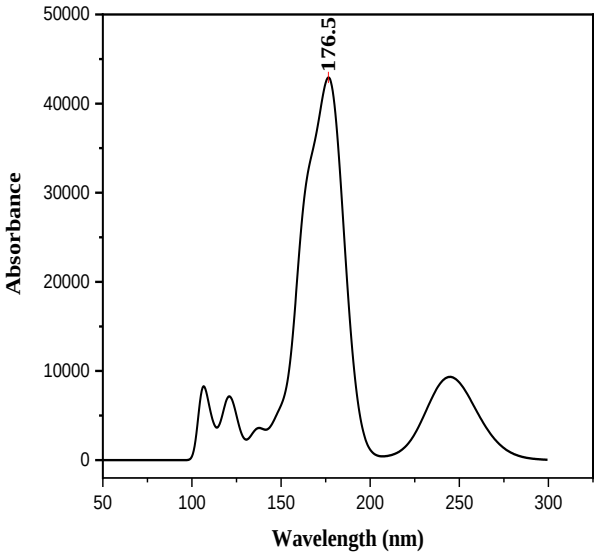

Figure 11: UV-Vis spectra with dichloro-ethane solvation

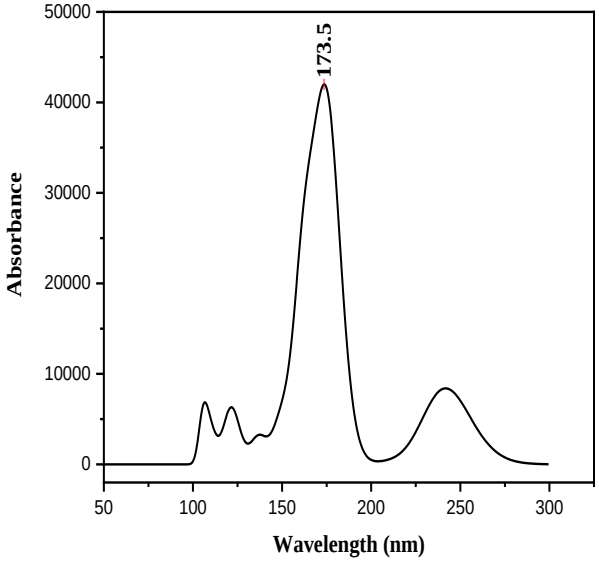

Figure 12: UV-Vis spectra with diethyl ether solvation

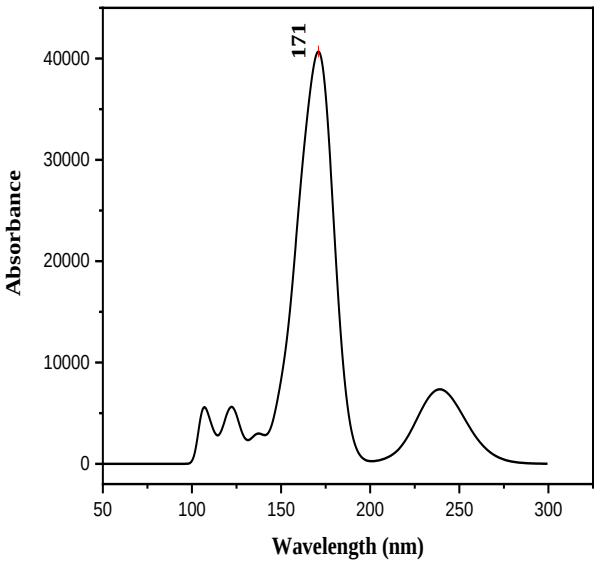

Figure 13: UV-Vis spectra with toluene solvation

4. Conclusion

In the present study, the theoretical analysis of DA has been performed to analyze the compounds included charge distribution, the results show that the atomies which was closed to nitrogen the charge is positive but the atomies which was closed to oxygen and the charge was negative. Also, the energy of the occupation of the orbitals was determined. It is important to found the properties of the molecules. The natural bond orbital analysis was found the lewis and non-lewis structure of the molecule. The result has shown the DA is lewis structure. According to natural hybrid orbital analysis, the DA molecule was higher geometrical optimized. As well, UV-Vis spectra which have the best designated with Gaussian function. It can be easily calculated and the individual peaks can be resolved correctly in very highly overlapped areas. It was noted here that there is the convergence state for DA molecules at excited state n=30. It is revealed that type solvents affect the electron transitions and hence the shape of UV-Vis spectra. The wavelength of the maximum peaks for DA molecule at n=30 through all solvation models (acetonitrile, chloroform, cyclohexane, dichloro-ethane, diethyl ether, and toluene) have appeared from 170 nm to 178.5 nm. Their numbers are close to each other but there is some shifting difference in their wavelengths.

REFERENCES

[1] L. Ahmed, R. OMER and H. Kebiroglu. A theoretical study on Dopamine molecule. Journal of Physical Chemistry and Functional Materials. 2019;2(2):66-72.

[2] M. Mehdizadeh Barforushi and K. Zare. A Theoretical Study on Dopamine: Geometry, energies and NMR. Journal of Physical & Theoretical Chemistry. 2014;11(2):57-61.

[3] S. J. Cragg, J. Baufreton, Y. Xue, J. P. Bolam and M. D. Bevan. Synaptic release of dopamine in the subthalamic nucleus. European Journal of Neuroscience. 2004;20(7):1788-1802.

[4] A. T. Gulledge and D. B. Jaffe. Dopamine decreases the excitability of layer V pyramidal cells in the rat prefrontal cortex. Journal of Neuroscience. 1998;18(21):9139-9151.

[5] T. Tzschentke. Pharmacology and behavioral pharmacology of the mesocortical dopamine system. Progress in neurobiology. 2001;63(3):241-320.

[6] H. Juárez Olguín, D. Calderón Guzmán, E. Hernández García and G. Barragán Mejía. The role of dopamine and its dysfunction as a consequence of oxidative stress. Oxidative medicine and cellular longevity. 2016;2016.

[7] R. Levy, P. Ashby, W. D. Hutchison, A. E. Lang, A. M. Lozano and J. O. Dostrovsky. Dependence of subthalamic nucleus oscillations on movement and dopamine in Parkinson's disease. Brain. 2002;125(6):1196-1209.

[8] M. M. Barforushi. NMR and NBO investigation of Dopamine properties in point view of Brain activities. Oriental Journal of Chemistry. 2014;30(4):1823-1840.

[9] B. Rubí and P. Maechler. Minireview: new roles for peripheral dopamine on metabolic control and tumor growth: let's seek the balance. Endocrinology. 2010;151(12):5570-5581.

[10] J.-H. Baik. Dopamine signaling in reward-related behaviors. Frontiers in neural circuits. 2013;7:152.

[11] R. Arreola, S. Alvarez-Herrera, G. Pérez-Sánchez, E. Becerril-Villanueva, C. Cruz-Fuentes, E. O. Flores-Gutierrez, M. E. Garcés-Alvarez, D. L. De La Cruz-Aguilera, E. Medina-Rivero and G. Hurtado-Alvarado. Immunomodulatory effects mediated by dopamine. Journal of immunology research. 2016;2016.

[12] T. G. Hastings. The role of dopamine oxidation in mitochondrial dysfunction: implications for Parkinson's disease. Journal of bioenergetics and biomembranes. 2009;41(6):469-472.

[13] H. Tost, T. Alam and A. Meyer-Lindenberg. Dopamine and psychosis: theory, pathomechanisms and intermediate phenotypes. Neuroscience & Biobehavioral Reviews. 2010;34(5):689-700.

[14] R. Franco, R. Pacheco, C. Lluis, G. P. Ahern and P. J. O'Connell. The emergence of neurotransmitters as immune modulators. Trends in immunology. 2007;28(9):400-407.

[15] S. Basu and P. S. Dasgupta. Dopamine, a neurotransmitter, influences the immune system. Journal of neuroimmunology. 2000;102(2):113-124.

[16] M. Cosentino and F. Marino. Adrenergic and dopaminergic modulation of immunity in multiple sclerosis: teaching old drugs new tricks? Journal of Neuroimmune Pharmacology. 2013;8(1):163-179.

[17] R. Pacheco, T. Gallart, C. Lluis and R. Franco. Role of glutamate on T-cell mediated immunity. Journal of neuroimmunology. 2007;185(1-2):9-19.

[18] K. F. Atkinson, S. H. Kathem, X. Jin, B. S. Muntean, W. A. Abou-Alaiwi, A. M. Nauli and S. M. Nauli. Dopaminergic signaling within the primary cilia in the renovascular system. Frontiers in physiology. 2015;6:103.

[19] R. Arreola, E. Becerril-Villanueva, C. Cruz-Fuentes, M. A. Velasco-Velázquez, M. E. Garcés-Alvarez, G. Hurtado-Alvarado, S. Quintero-Fabian and L. Pavón. Immunomodulatory effects mediated by serotonin. Journal of immunology research. 2015;2015.

[20] Y. Zhang, S. Cuevas, L. D. Asico, C. Escano, Y. Yang, A. M. Pascua, X. Wang, J. E. Jones, D. Grandy and G. Eisner. Deficient dopamine D2 receptor function causes renal inflammation independently of high blood pressure. PLoS One. 2012;7(6).

[21] D. C. Borcherding, E. R. Hugo, G. Idelman, A. De Silva, N. W. Richtand, J. Loftus and N. Ben-Jonathan. Dopamine receptors in human adipocytes: expression and functions. PLoS One. 2011;6(9).

[22] R. S. Othman, R. A. Omar, K. A. Omar, A. I. Gheni, R. Q. Ahmad, S. M. Salih and A. N. Hassan. Synthesis of Zinc Sulfide Nanoparticles by Chemical Coprecipitation Method and its Bactericidal Activity Application. Polytechnic Journal. 2019;9(2):156-160.

[23] E. Nagy, I. Berczi, G. E. Wren, S. L. Asa and K. Kovacs. Immunomodulation by bromocriptine. Immunopharmacology. 1983;6(3):231-243.

[24] J. Bergquist, A. Tarkowski, R. Ekman and A. Ewing. Discovery of endogenous catecholamines in lymphocytes and evidence for catecholamine regulation of lymphocyte function via an autocrine loop. Proceedings of the National Academy of Sciences. 1994;91(26):12912-12916.

[25] M. Levite. Nerve-driven immunity. The direct effects of neurotransmitters on T-cell function Ann NY Acad Sci. 2000;917:307-321.

[26] I. Berczi, A. Quintanar-Stephano and K. Kovacs. Neuroimmune regulation in immunocompetence, acute illness, and healing. Annals of the New York Academy of Sciences. 2009;1153(1):220-239.

[27] R. A. Vaughan and J. D. Foster. Mechanisms of dopamine transporter regulation in normal and disease states. Trends in pharmacological sciences. 2013;34(9):489-496.

[28] A. Asthagiri and M. Janik. Computational catalysis. Royal Society of Chemistry; 2014.

[29] F. M. AVCU and M. Karakaplan. Finding Exact Number Of Peaks in Broadband UV-Vis Spectra Using Curve Fitting

Method Based On Evolutionary Computing. Journal of the Turkish Chemical Society Section A: Chemistry. 2020;7(1):117-124.
[30] R. A. Omer, A. Hughes, J. R. Hama, W. Wang and H. Tai. Hydrogels from dextran and soybean oil by UV photo-polymerization. Journal of Applied Polymer Science. 2015;132(6).
[31] R. J. Anderson, D. J. Bendell and P. W. Groundwater. Organic spectroscopic analysis. Royal Society of Chemistry; 2004.
[32] H. Tanak, A. Ağar and M. Yavuz. Combined experimental and computational modeling studies on 4-[(2-hydroxy-3-methylbenzylidene) amino]-1, 5-dimethyl-2-phenyl-1, 2-dihydro-3H-pyrazol-3-one. International Journal of Quantum Chemistry. 2011;111(9):2123-2136.
[33] E. McRae. Theory of solvent effects on molecular electronic spectra. Frequency shifts. The Journal of Physical Chemistry. 1957;61(5):562-572.
[34] W. Freitag and D. Stoye. Paints, coatings and solvents. John Wiley & Sons; 2008.
[35] Z. Ul-Haq and J. D. Madura. Frontiers in Computational Chemistry: Volume 2: Computer Applications for Drug Design and Biomolecular Systems. Elsevier; 2015.
[36] A. Ayeshamariam, S. Ramalingam, M. Bououdina and M. Jayachandran. Preparation and characterizations of SnO2 nanopowder and spectroscopic (FT-IR, FT-Raman, UV–Visible and NMR) analysis using HF and DFT calculations. Spectrochimica Acta Part A: Molecular and Biomolecular Spectroscopy. 2014;118:1135-1143.
[37] S. Gunasekaran, R. A. Balaji, S. Kumeresan, G. Anand and S. Srinivasan. Experimental and theoretical investigations of spectroscopic properties of N-acetyl-5-methoxytryptamine. Can. J. Anal. Sci. Spectrosc. 2008;53(4):149-162.
[38] K. Sarikavak and F. Sevin. Structural and Spectral (IR, NMR and UV/Visible) Properties of Newly Designed Boronic Acid Derivatives Containing DO3A Sensitive to Uranyl Ion: A DFT and TD-DFT Study. Computational Chemistry. 2017;5(4):145-158.
[39] H. Tanak, A. A. Ağar and O. Büyükgüngör. Experimental (XRD, FT-IR and UV–Vis) and theoretical modeling studies of Schiff base (E)-N′-((5-nitrothiophen-2-yl) methylene)-2-phenoxyaniline. Spectrochimica Acta Part A: Molecular and Biomolecular Spectroscopy. 2014;118:672-682.
[40] N. ÖZTÜRK, H. GÖKCE, G. ALPASLAN, Y. B. ALPASLAN and C. ALAŞALVAR. Structural, Spectroscopic (FT-IR, Raman, NMR and UV-Vis.) and Computational Studies on N-phenylpropanamide. Iğdır Üniversitesi Fen Bilimleri Enstitüsü Dergisi.9(2):823-834.
[41] C. Sangeetha, R. Madivanane and V. Pouchaname. The Vibrational Spectroscopic (FT-IR & FT Raman, NMR, UV) Study and HOMO & LUMO Analysis of Phthalazine by DFT and HF Studies. International Journal Of Engineering Research and General Science. 2014;2:222.
[42] H. Mohammad-Shiri, M. Ghaemi, S. Riahi and A. Akbari-Sehat. Computational and electrochemical studies on the redox reaction of dopamine in aqueous solution. Int. J. Electrochem. Sci. 2011;6:317-336.
[43] J. Argüello, V. L. Leidens, H. A. Magosso, R. R. Ramos and Y. Gushikem. Simultaneous voltammetric determination of ascorbic acid, dopamine and uric acid by methylene blue adsorbed on a phosphorylated zirconia–silica composite electrode. Electrochimica Acta. 2008;54(2):560-565.
[44] N. Karthikeyan, J. J. Prince, S. Ramalingam and S. Periandy. Electronic [UV–visible] and vibrational [FT-IR, FT-Raman] investigation and NMR–mass spectroscopic analysis of terephthalic acid using quantum Gaussian calculations. Spectrochimica Acta Part A: Molecular and Biomolecular Spectroscopy. 2015;139:229-242.
[45] I. Georgieva, N. Danchova, S. Gutzov and N. Trendafilova. DFT modeling, UV-Vis and IR spectroscopic study of acetylacetone-modified zirconia sol-gel materials. Journal of molecular modeling. 2012;18(6):2409-2422.
[46] F. Parveen, T. Patra and S. Upadhyayula. Hydrolysis of microcrystalline cellulose using functionalized Bronsted acidic ionic liquids–A comparative study. Carbohydrate polymers. 2016;135:280-284.
[47] A. Pietrzyk, S. Suriyanarayanan, W. Kutner, E. Maligaspe, M. E. Zandler and F. D'Souza. Molecularly imprinted poly [bis (2, 2′-bithienyl) methane] film with built-in molecular recognition sites for a piezoelectric microgravimetry chemosensor for selective determination of dopamine. Bioelectrochemistry. 2010;80(1):62-72.
[48] F. M. AVCU and M. Karakaplan. Finding Exact Number Of Peaks in Broadband UV-Vis Spectra Using Curve Fitting Method Based On Evolutionary Computing. Journal of the Turkish Chemical Society Section A: Chemistry.7(1):117-124.
[49] K. SAYIN. Computational Investigations on IR, UV-VIS and NMR Spectra of Copper (II) Phenanthroline Complexes with DFT Method. Cumhuriyet Science Journal. 2017;38(4):661-673.
[50] C. Zhai, D. Li, L. Li, F. Sun, H. Ma and X. Liu. Experimental and theoretical study on the hydrogen bonding between dopamine hydrochloride and N, N-dimethyl formamide. Spectrochimica Acta Part A: Molecular and Biomolecular Spectroscopy. 2015;145:500-504.
[51] R. A. Omer, J. R. Hama and R. S. M. Rashid. The effect of dextran molecular weight on the biodegradable hydrogel with oil, synthesized by the michael addition reaction. Advances in Polymer Technology. 2017;36(1):120-127.
[52] R. M. A. Idris, E. A. Gadkariem, K. E. I. M. A. Mohamed and M. E. Hagga. Kinetic Method for Determination of Dopamine HCl in Bulk & Injectable Forms. International Journal of Chemical Science and Technology. 2011;2(2):218-223.
[53] A. W. Ravna, I. Sylte and S. G. Dahl. Molecular model of the neural dopamine transporter. Journal of computer-aided molecular design. 2003;17(5-6):367-382.
[54] L. A. OMER and O. Rebaz. Computational Study on Paracetamol Drug. Journal of Physical Chemistry and Functional Materials. 2020;3(1):9-13.
[55] R. OMER, P. KOPARIR, L. AHMED and M. KOPARIR. Computational determination the reactivity of salbutamol and propranolol drugs. Turkish Computational and Theoretical Chemistry. 2020;4(2):67-75.
[56] İ. Sıdır, Y. G. Sıdır, M. Kumalar and E. Taşal. Ab initio Hartree–Fock and density functional theory investigations on the conformational stability, molecular structure and vibrational spectra of 7-acetoxy-6-(2, 3-dibromopropyl)-4, 8-dimethylcoumarin molecule. Journal of Molecular Structure. 2010;964(1-3):134-151.
[57] K. Jug and Z. B. Maksić. The Meaning and Distribution of Atomic Charges in Molecules. Theoretical Models of Chemical Bonding. Springer; 1991. p. 235-288.